

ARTICLE

Open Access

# Streaming-based Tweezers for Routing, Engineering, and Manipulation of multiparticles: STREAM

Haodong Zhu<sup>1</sup>, Wenjun Yu<sup>1</sup>, Neil Upreti<sup>2</sup> and Tony Jun Huang<sup>1</sup>✉

## Abstract

Contactless manipulation of samples, particularly the ability to dynamically handle multiple fragile specimens while maintaining their integrity and viability, is crucial for various applications in biology, medicine, engineering, and physics. While hydrodynamic tweezers have emerged as a promising approach for gentle, label-free manipulation of a wide range of sample types and sizes, they typically have limited flexibility in terms of dynamic control, making it challenging to realize high-resolution and programmable manipulation of multiple samples. Here, we introduce the Streaming-based Tweezers for Routing, Engineering, And Manipulation of multiparticles (STREAM) with sub-wavelength resolution. The platform employs an array of piezoelectric plates arranged in a space-reciprocal pattern to generate acoustic streaming, creating localized trapping points. The mechanism of particle trapping and the improvement of routing resolution via multiunit activation were investigated. Subsequently, a convolutional neural network (CNN) with arbitrary voltage combination as the input and predicted trapping position as the output was integrated into the system. The CNN calibration is vital to the system as it enhances the platform's performance, enabling precise control of the trapping positions beyond traditional physical unit size limitations. We demonstrated the STREAM platform's capabilities through single particle routing with sub-wavelength precision, simultaneous manipulation of multiple particles, and on-demand assembly of samples. The STREAM platform opens new possibilities for applications requiring precise and dynamic control of particles and samples, with the potential to advance fields including biology, chemistry, and materials science.

## Introduction

Contactless manipulation of samples is crucial for various applications in fields such as biology and material science. In particular, the ability to handle fragile samples without physical contact is highly desirable to maintain integrity and viability. For instance, in the study of zebrafish larvae, a popular vertebrate model organism, gentle manipulation is crucial to avoid inducing stress or injury that could affect their development and behavior<sup>1,2</sup>. Contactless manipulation also enables the positioning and

orientation of samples, such as protein crystals, for imaging or analysis without introducing mechanical disturbances<sup>3–5</sup>. Furthermore, the dynamic manipulation of multiple samples in a contactless manner is of paramount importance for high-throughput applications<sup>6–10</sup>, such as drug screening<sup>11</sup>, where the ability to efficiently handle and analyze numerous samples simultaneously can greatly accelerate the discovery and development of novel therapeutics<sup>12,13</sup>.

During the past years, various contactless manipulation techniques have been developed. Among them, optical tweezers use focused laser beams to trap and manipulate small objects precisely but require complex instrumentation and may cause photodamage<sup>14–19</sup>. Magnetic tweezers use magnetic fields to manipulate particles with magnetic properties or tags, offering good biocompatibility but

Correspondence: Tony Jun Huang (tony.huang@duke.edu)

<sup>1</sup>Department of Mechanical Engineering and Material Science, Duke University, Durham, NC 27708, USA

<sup>2</sup>Department of Biomedical Engineering, Duke University, Durham, NC 27708, USA

© The Author(s) 2025



**Open Access** This article is licensed under a Creative Commons Attribution-NonCommercial-NoDerivatives 4.0 International License, which permits any non-commercial use, sharing, distribution and reproduction in any medium or format, as long as you give appropriate credit to the original author(s) and the source, provide a link to the Creative Commons licence, and indicate if you modified the licensed material. You do not have permission under this licence to share adapted material derived from this article or parts of it. The images or other third party material in this article are included in the article's Creative Commons licence, unless indicated otherwise in a credit line to the material. If material is not included in the article's Creative Commons licence and your intended use is not permitted by statutory regulation or exceeds the permitted use, you will need to obtain permission directly from the copyright holder. To view a copy of this licence, visit <http://creativecommons.org/licenses/by-nc-nd/4.0/>.

requiring the introduction of magnetic materials which may not be suitable for all applications. In contrast, acoustic streaming-based hydrodynamic tweezers have emerged as a promising approach for contactless manipulation, offering the advantage of gentle, label-free handling and compatibility with a wide range of sample types and sizes<sup>20–27</sup>. The platforms based on oscillating bubbles, for example, generate vortices for particle trapping and manipulation, allowing for contactless manipulation; however, this method cannot precisely control the trapping position or motion of particles<sup>28–31</sup>. Of further note, programmable manipulation of single or multiple particles has been realized in several acoustic streaming-based platforms<sup>32–35</sup>. However, their setup always relies on the Chladni patterns on a vibrating substrate, resulting in direct contact of the particle manipulated with the substrate and a low level of spatial accuracy for single particle manipulation. While other acoustic streaming-driven devices have also been explored, they typically operate at fixed frequencies and have limited flexibility in terms of dynamic control<sup>36–46</sup>. Until now, hydrodynamic-based contactless multiparticle manipulation with high resolution and programmability has remained a significant challenge.

In this article, we introduce the Streaming-based Tweezers for Routing, Engineering, And Manipulation of multiparticles (STREAM) with high programmability and sub-wavelength resolution. By selectively activating specific combinations of piezoelectric plates with different input voltage combinations using a dynamic multi-channel controlling method, we can create localized trapping points at any point in the  $x$ – $y$  plane, enabling dynamic manipulation of multiple particles along complex arbitrary routes simultaneously. Furthermore, the platform's performance is enhanced by integrating a convolutional neural network (CNN) that enables precise prediction and control of the trapping positions, overcoming the limitations imposed by the physical size of the STREAM units (0.2 mm resolution for the unit size of 6 mm). After demonstrating the STREAM platform's capabilities in single particle routing with improved precision (<0.2 mm for 1 mm particles) with multiple arbitrary shapes, we moved on to demonstrate the simultaneous manipulation of multiple particles along arbitrary routes, as well as the on-demand assembly of multiple samples into arbitrary shapes. The STREAM platform, with its unique capability to achieve contactless and dynamic manipulation of multiple samples simultaneously, surpasses the limitations of previous acoustic streaming-based hydrodynamic tweezer platforms, while also demonstrating biocompatibility for handling fragile biological samples (see the “Materials and methods” section). The advancement opens up new possibilities for applications requiring precise and

dynamic control of particles and samples, such as drug screening, controlled crystallization, acoustic-based sensing and microassembly<sup>47–51</sup>.

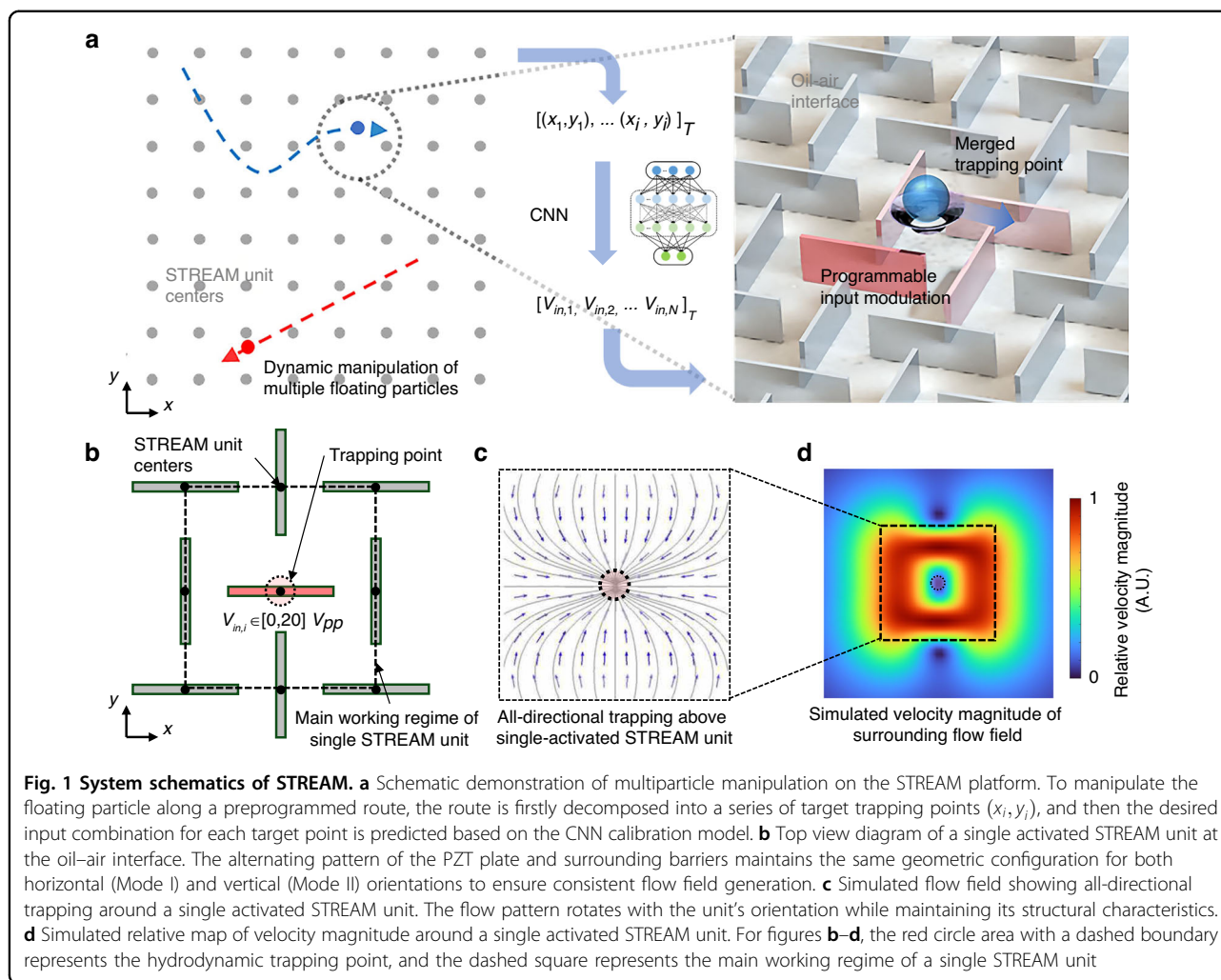
## Results

### Mechanism of particle trapping in the STREAM platform

As shown in Fig. 1a, the STREAM platform consists of an array of square-shaped upright piezoelectric transducer (PZT) plates arranged in a space-reciprocal pattern (as shown in Fig. 1b), with each upright PZT plate constituting a STREAM unit. The geometry of each unit (and the patterning surrounding it) is congruent, with one pattern being perpendicular to the unit geometry adjacent to it. The entire platform is submerged in the carrier oil, FC-40, to control the position of multiple particles or other samples floating at the oil–air interface (see the “Materials and methods” section). Each PZT plate, along with the other plates surrounding it, forms the space-reciprocal pattern and is considered a functional STREAM unit.

The reciprocal space pattern surrounding the STREAM unit, as illustrated in Fig. 1b, is pivotal in generating the omnidirectional trapping effect. Rotating the STREAM unit modifies the orientation but not the structure of its flow field. As a result, the entire flow pattern rotates in accordance with the orientation of the unit, while preserving its fundamental characteristics. For instance, when the PZT plate within the unit is oriented horizontally (Unit Mode I), it generates the flow field pattern shown in Fig. 1c with velocity magnitudes as depicted in Fig. 1d. When the unit is rotated 90° to its vertical orientation (Unit Mode II), the same flow field pattern is generated but rotated accordingly—effectively creating an identical flow structure rotated 90° from the Mode I configuration. In both cases, the spatial distribution of velocities and the overall trapping characteristics remain structurally identical, with only their orientation changing to match that of the generating unit.

When activated with a radio-frequency signal at a specific time point,  $V_{in,i}$  (11.2 MHz, 0–20 Vpp), the acoustic streaming generated by the vibrating PZT plate will be shaped by the surrounding barrier structures. Due to Kelvin–Helmholtz instability<sup>52</sup>, the acoustic streaming will form a pair of horseshoe-shaped vortex beams with opposite vorticity on each side of the vibrating PZT plate, ensuring that regardless of the unit's orientation, the flow field creates attraction forces toward the center of the unit from all eight adjacent units (the region marked by black dotted line in Fig. 1c and d). These vortex pairs interact with the surrounding barrier structure to generate stable streaming patterns that converge at the center of the unit, resulting in a robust omnidirectional trapping point at the oil–air interface on a time scale of <100 ms that persists regardless of the unit's rotational alignment.



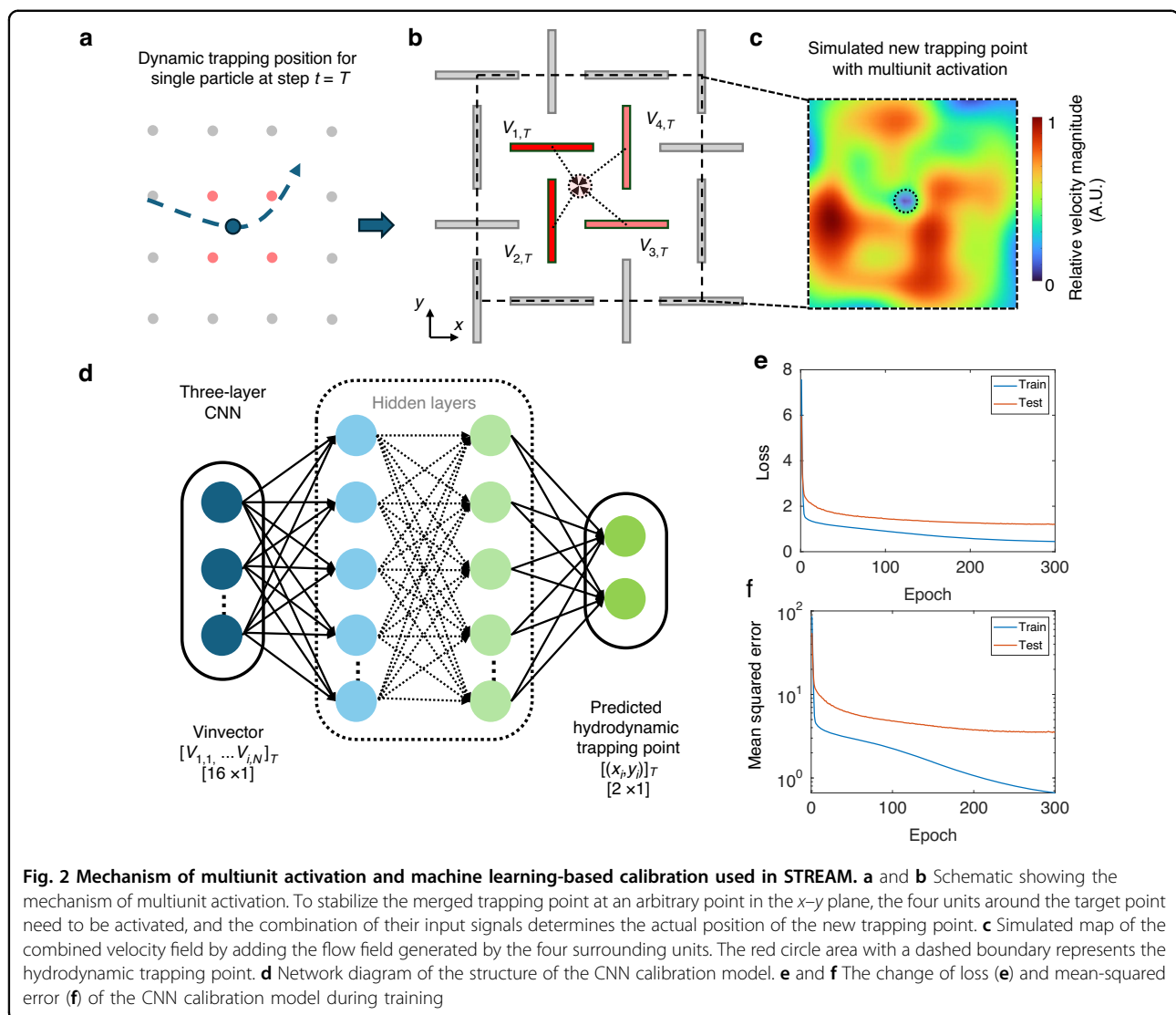
Following a simplified model utilizing the Biot–Savart Law and simplifying the 3D flow field into segments of vortex tubes<sup>53</sup>, we get an estimation of the flow field generated on the oil–air interface (Fig. 1c and d, with Unit Mode I as an example). Based on the simulation results of the flow field, we see that the trapping effect extends further in the  $x$  direction, and the radial velocity, which creates the trapping effect, changes more rapidly in the  $y$  direction. In both the  $x$  and  $y$  directions, the region of higher velocity (represented by the red area in Fig. 1d) primarily extends to the eight units surrounding the activated unit, as indicated by the area inside the dashed line in Fig. 1c and d. This observation makes it reasonable to assume that the “main working regime” of a single activated STREAM unit is the square area marked by the centers of the eight units surrounding it.

Meanwhile, because of the millimeter scale of the STREAM units and the high viscosity of the carrier oil as the liquid environment, the Reynold number ( $Re$ ) of the platform falls in the laminar flow regime ( $Re \sim O(1)$ ).

The linearity of the whole flow system yields two reasonable assumptions that help validate the feasibility of high-precision trapping with multiple STREAM units. First, the trapping flow field generated by a single STREAM unit, along with its omnidirectional trapping characteristics, can be maintained under varying voltage inputs. With enough input energy to build up a steady flow field, one that can allow the vortex tube to reach the oil–air interface ( $6\text{--}20 V_{pp}$ ), only the trapping strength (i.e., the overall velocity magnitude of the trapping flow field) is correlated with voltage inputs. Second, since we believe that the platform operates in the laminar regime, the flow field contribution of multiple units can possibly be predicted by simply adding linearly.

#### Improving the routing resolution of the STREAM via multiunit activation

When activating two adjacent STREAM units, the flow field generated by each unit will pull the floating particle to its center, resulting in a new merged trapping point in



the middle of the two units. To prove the possibility of multiunit activation experimentally, we perform a testing experiment with one solid polystyrene particle (1  $\mu\text{m}$  in diameter) and a varying input voltage ratio between two adjacent STREAM units. As the input voltage ratio of Unit 2 over Unit 1,  $V_{2,T}/V_{1,T}$ , gradually increases, the merged trapping point gradually and continuously shifts from the center of Unit 1 to the center of Unit 2 (Supplementary Fig. 1).

This gradual change of merged trapping points highlights the feasibility of high-resolution particle manipulation by simply tuning the input ratio of the activated units. Unlike the previous acoustohydrodynamic tweezers setup<sup>53</sup>, which was limited to ON/OFF modes, thereby constraining spatial resolution to the physical size of the unit (e.g., 6  $\mu\text{m}$ ), our approach allows for particle trapping at any point in the  $x$ - $y$  plane by adjusting the input voltages of the four units surrounding the trapping point

(Fig. 2a). As shown in Fig. 2b, if we activate the four adjacent STREAM units at the same time with independent inputs (where the denser red color represents a higher voltage), the combined flow field will form a new trapping point in the middle of these four units, which is closer to the unit(s) with high inputs (Fig. 2c). This new control mechanism enables the STREAM platform to perform more complex and programmable particle manipulation scenarios.

However, predicting the precise position of the merged trapping point is more challenging than simply combining the simulation results. The main obstacles are twofold. First, there is no direct relationship between the input voltage and the magnitude of the velocity generated by each unit. Despite the existence of methods such as particle image velocimetry to measure the velocity magnitude of certain flow fields, there is an overwhelming workload to scan all the units with sufficiently varying inputs. More



importantly, although our simulations assume that all STREAM units are identical (regardless of Mode I or II), this is not the case in practice. Fabrication variability of each PZT plate leads to deviations in the actual trapping position and the generated velocity.

To overcome this challenge to obtain a more accurate prediction of the trapping position, we use a machine learning-based calibration model with CNN. As shown in Fig. 2d, the neural network consists of three hidden layers. We use the combination of the input voltage of each unit (e.g., a  $16 \times 1$  vector for the  $4 \times 4$ -unit prototype used in this work) as the model input and use the stable position of the combined hydrodynamic trapping point as the model output. We use a training set containing  $\sim 6000$  different combinations of inputs spanning over different units and a random 10% portion of the training set for validation. As shown in Fig. 2e and f, the model is trained after  $\sim 300$  iterations, and the mean error of the predicted trapping point stabilizes at around 0.5 mm, with the error representing the addition of error in both  $x$  and  $y$ . As the last step to predict the results of an input voltage combination and its output trapping point  $(x_i, y_i)$ , we start from a position in the training set that is close to the position  $(x_i, y_i)$ , and then use the trained model to scan around the training set input to get the input vector with minimal spatial loss. For a more detailed discussion of the CNN model or the training and predicting process (see the “Materials and methods” section).

### Single particle routing via STREAM

With the CNN calibration model setup, we perform a tracing experiment to demonstrate the improved trapping precision introduced by the model (Supplementary Movie 1). Here, we designed a target trace with a spiral shape, starting from the center of the prototype platform and ending at the middle point of the right side (Table S1). The spiral trace is described in radial coordinates and then decomposed into a series of 40 individual target points, with the step size  $\Delta\theta = \pi/20$ . We tested three different approaches to predict the ideal input to trace a spiral with the red polystyrene particle (1 mm in diameter). The three approaches were simulation alone (Fig. 3a, i), using the input combination of the closest point to the target from the training set (Fig. 3a, ii), and using the prediction of the CNN model (Fig. 3a, iii). As expected, the results clearly show that the trace generated by simulation alone has some trapping positions far away from the target points, and the prediction based on the CNN model generates the best tracing performance of all three approaches.

We then use the CNN prediction method to test another circle-shaped enclosed trace (Table S1). Similarly, the trace is described in radial coordinates and then decomposed into 40 separate target points, with the step

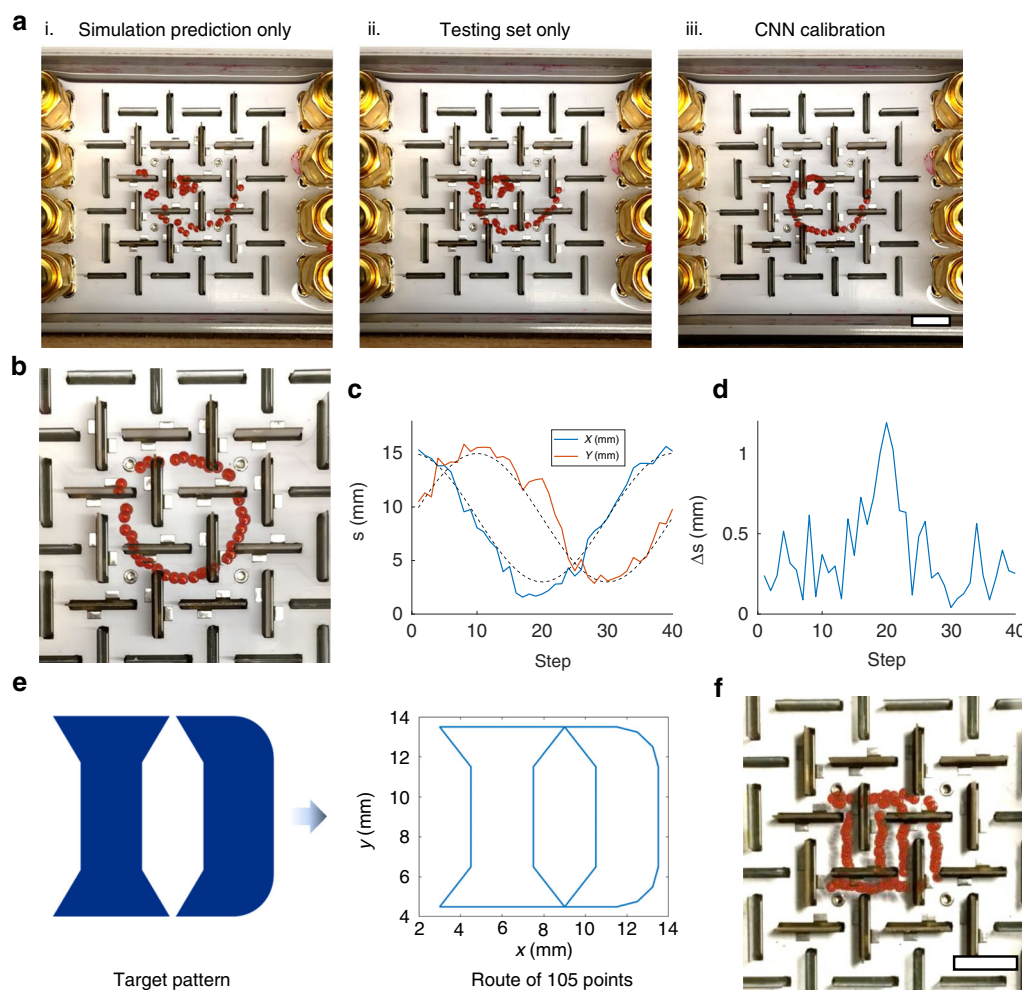
size  $\Delta\theta = \pi/20$ . Similar to Fig. 3a, iii, the time stack of trapping positions at each time step in Fig. 3b demonstrates strong tracking performance. Figure 3c illustrates the actual trapping position at each step in both the  $x$  and  $y$  directions, while Fig. 3d presents the relative error at each step. Compared to the target point, we can prove that the average error of trapping along an arbitrary trace is on the sub-millimeter scale, which is much smaller than the scale of the STREAM unit itself and fits well with the result from the machine learning model.

Figure 3e and Supplementary Fig. 2c both show another example with a more complicated route (shaped like the letter “D”) which is decomposed into a series of 105 individual points. The time-stacked result in Fig. 3f shows similar spatial accuracy performance compared to the previous routes, demonstrating the capability of the STREAM platform to perform complicated routing of single particles.

### Routing of multiple particles via STREAM

After demonstrating the tracing of a single particle with sub-wavelength spatial resolution, we elaborate on the idea of controlling multiple particles simultaneously. As mentioned earlier, the primary working regime of a single STREAM unit only extends to its surrounding units. Thus, if the square area formed by  $2 \times 2$  centers of adjacent STREAM units is considered a “block,” two trapping points can coexist as long as they are not located in adjacent blocks, as the flow field forming at each point will not cause significant interference. By simply adding up the input vector needed to generate such two points separately, we can trap two particles at different places at once.

In addition to this scenario, we tested a square-shaped route with the synchronized control of two particles (Fig. 4a and Supplementary Movie 2). For each particle, the traces are described in cartesian coordinates and then decomposed into 21 individual target points, with a step size of 1 mm. The two polystyrene particles (1.5 mm in diameter) are set to be attracted at the opposite side of the center of the platform. Figure 4b, c shows the actual trapped position of the two particles in the  $x$  and  $y$  directions, respectively, with the dotted lines representing the target position in both the  $x$  and  $y$  directions. Meanwhile, Fig. 4d shows the spatial error for each step for both trapped particles, respectively. Although the spatial error is about two times higher than single particle tracing, it is still much smaller than the scale of a single unit, proving the feasibility of routing multiple particles with high resolution in the STREAM platform. Figure 4e shows the time stack image of the trapping positions for an individual particle at each time step, respectively. In contrast, Fig. 4f, i–vii shows the actual position of the two trapped particles at seven different timeframes.



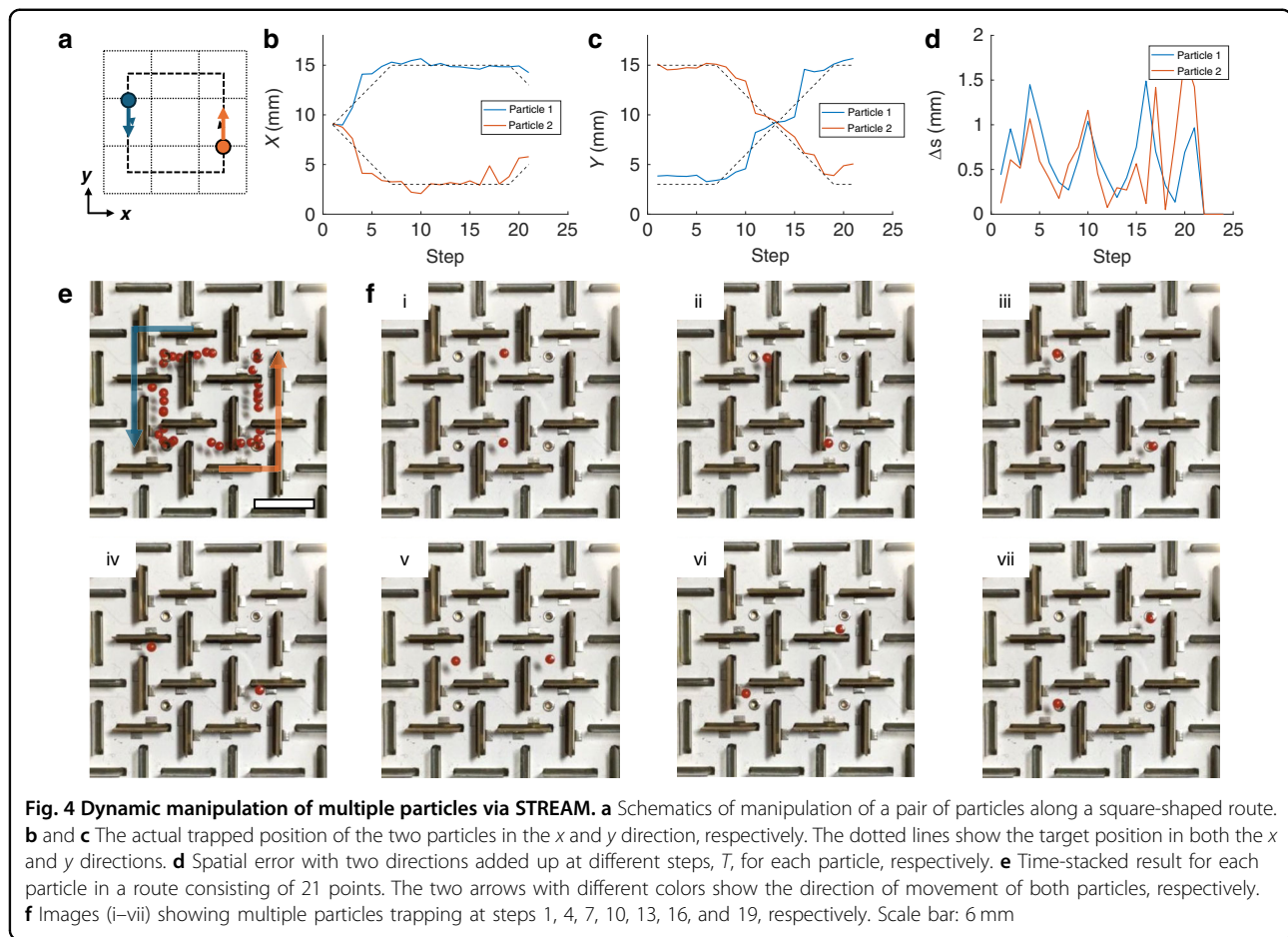
**Fig. 3 Dynamic routing of a single particle via STREAM.** **a** Time-stacked result of a spiral-shaped route with (i) simulation only, (ii) the input combination of the closest point to the target from the training set only, and (iii) with the prediction of the CNN-based calibration model. **b** Time-stacked result of a circle-shaped route consisting of 40 points. **c** Actual position of trapping point in both  $x$  direction (blue line) and  $y$  direction (orange line) at different steps,  $T$ . **d** Combined  $x$ - $y$  spatial error with a varying number of steps,  $T$ . **e** The “D” shaped route with 105 points. **f** Time-stacked result of the D-shaped route consisting of 105 points. Scale bars: 6 mm

### On-demand assembly via dynamic control signals of STREAM

As a further test of the dynamic manipulation capability of the STREAM platform, we perform a more complicated control scenario to perform a step-based assembly to create different Tetris-like shapes. Four thin rectangular prisms made of Polydimethylsiloxane (PDMS) (with the size of  $\sim 3 \times 3 \times 1 \text{ mm}^3$ ) are used as the unit block to form the Tetris-like shapes. Figure 5a shows the general process to produce an assemblage of a specific shape. For each scenario, the four PDMS unit blocks are first trapped at the four corner units of the platform, and two unit blocks on the right are released and assembled near the center of the platform, as shown in the output of the initialization step in Fig. 5b. The next two steps of assembly are considered “Dynamic Control Steps,” during

which a unit block at the upper-left corner and the bottom-left corner is added to the assemblage one at a time. By tuning an input combination of the eight STREAM units on the left side of the platform during these two steps, we ascertain the dynamic flow field that dictates the orientation of the assembly when it combines with another block and determines the result of the assembly.

Based on both flow field simulation and corresponding testing experiments with different input combinations, we find four groups of input combinations consistently leading to four different Tetris-like shapes, respectively. Figure 5c lists the results forming four different target Tetris-like shapes, namely the “I-shape,” “Z-shape,” “L-shape,” and “T-shape” (Supplementary Movie 3). The simulated combined flow field for Dynamic Control Steps



I and II is listed for each shape. It is notable that the input combination at each step determines the shape and orientation of an assemblage. For example, the Dynamic Control Steps I of “I-shape” and “T-shape” both create an assemblage with three blocks in a row. Still, the input combination in the “T-shape” scenario creates an asymmetric flow field, leading to a tilted assemblage that will help the next block connect to the middle of it during the next step. This simple demonstration of dynamic assembly further proves the capability of the STREAM platform to perform dynamic control of multiple objects with multiunit-based control signals.

## Discussion and conclusion

In this work, we introduce the STREAM platform as a powerful tool for dynamic multiparticle manipulation with sub-wavelength resolution. By harnessing acoustic streaming generated by an array of piezoelectric plates and integrating a CNN, the STREAM platform enables precise and controllable manipulation of particles and samples, surpassing the limitations of the physical unit size. Experiments demonstrate the platform’s capabilities in single particle routing, simultaneous manipulation of multiple particles, and on-demand assembly of samples.

To further enhance the capabilities of the STREAM platform, future research will focus on miniaturizing individual units while increasing their overall number. While the current prototype operates at the millimeter scale with a Reynolds number ( $Re$ ) of order  $O(1)$ , scaling down the size of individual units will only decrease the  $Re$  further. This preserves the linear characteristics of the platform, ensuring that the system setup and control methods we’ve developed to achieve high-precision manipulation will remain effective for smaller-scale STREAM-based platforms. Notably, miniaturization would offer additional benefits beyond enhanced spatial resolution, including a reduction in the power required for unit actuation as the active area of the piezoelectric elements decreases. On the other hand, scaling up the number of units and miniaturizing each unit could allow the STREAM platform to manipulate smaller particles and handle more particles simultaneously. Such scaling advantages could enable the development of high-density arrays capable of manipulating particles at microscale dimensions, though achieving this will require overcoming current fabrication constraints.

Meanwhile, future improvements could focus on optimizing the actuation system for faster response times. The



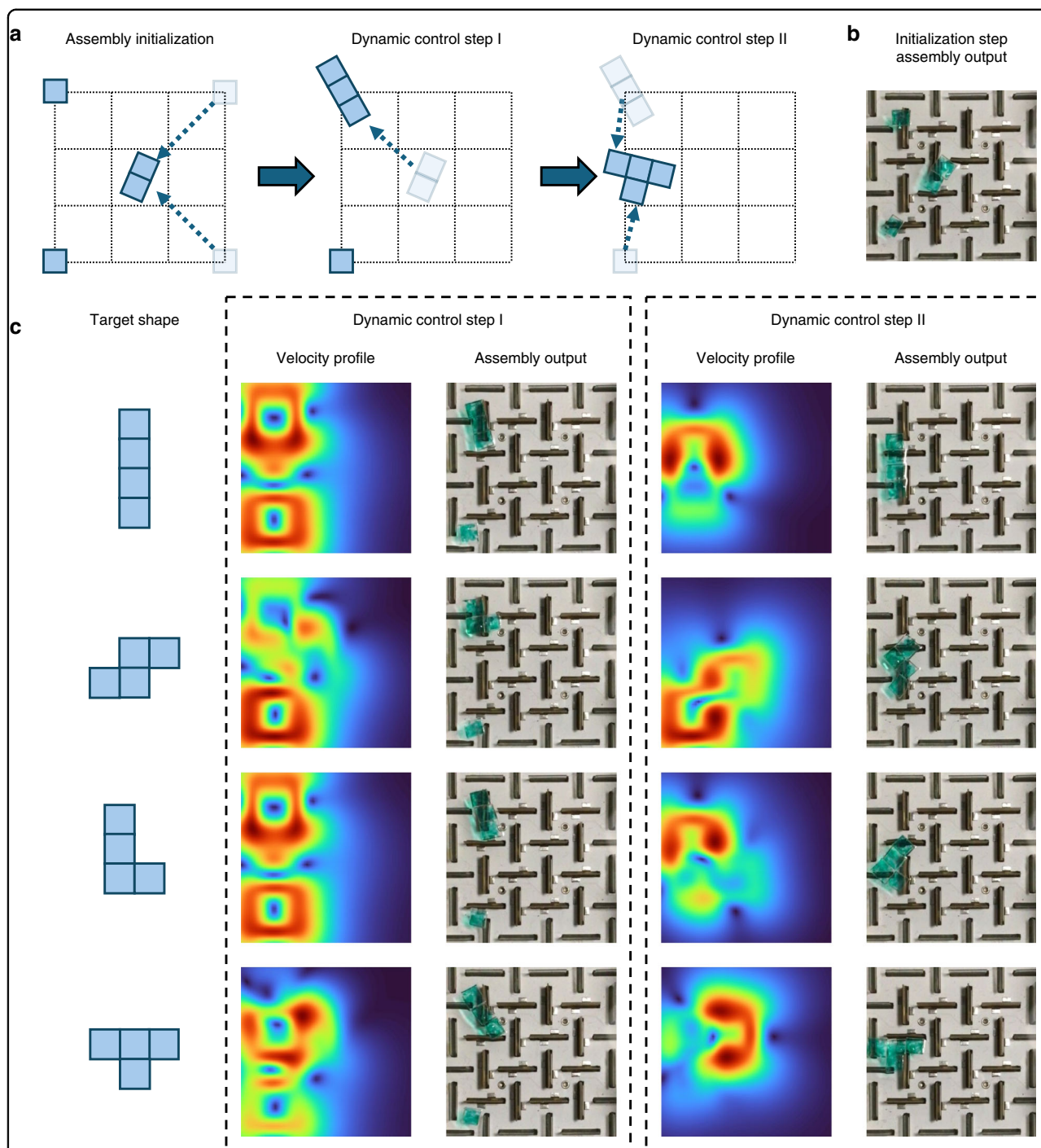


**Fig. 5** On-demand dynamic assembly via STREAM platform. **a** Schematics showing the process of dynamic assembly. The four PDMS unit blocks are first trapped at the four corner units of the platform, and the two-unit blocks on the right are both released and connected near the center of the platform. During the two successive “Dynamic Control Steps,” the unit blocks at the upper and bottom left corners are added to the assembly one at a time. **b** Experimental results showing various assemblages after the Initialization step. **c** List of the four different target shapes, the relative simulated velocity profile for each dynamic control step for each shape, and the corresponding experimental result of the assembly. Scale bar: 6 mm

current implementation uses multichannel function generators that introduce brief transient responses during voltage transitions, necessitating a 10-s step time to ensure stable particle positioning (see the “Materials and

methods” section). This operational constraint could be addressed through alternative hardware configurations, such as implementing individual fixed-gain power amplifiers or developing custom PCB-based multichannel



voltage control systems. Such engineering optimizations could significantly reduce the step time while maintaining the platform's precise manipulation capabilities. In particular, given that our platform operates at relatively low input voltages and typically requires <50% of units to be activated simultaneously, a modularized PCB-based approach would not only improve response time but also provide a practical solution for scaling up the number of units while maintaining a reasonable cost structure. These technical refinements, combined with the potential for miniaturization, would further expand the platform's applications in fields requiring high-throughput, dynamic particle manipulation.

With the proposed advancements in actuation systems and scalable design, the STREAM platform holds the potential to revolutionize high-throughput applications through automated parallel processing of multiple sample arrays. This capability could transform workflows in fields such as rapid drug screening, enabling simultaneous testing of numerous drug–cell interactions, and automated chemical detection assays with parallelized sample processing. Additionally, it could enhance protein crystal array analysis by facilitating precise particle and droplet manipulation, as well as controlled merging. Leveraging its sub-wavelength resolution and exceptional versatility, the STREAM platform could redefine precise micromanipulation, unlocking groundbreaking opportunities across a wide range of scientific and industrial domains.

## Materials and methods

### Fabrication and setup of the STREAM platform

The PZTs that constitute a STREAM unit have dimensions of 7 mm × 7 mm × 0.2 mm (SMPL7W7T02412, STEM Inc., FL, USA). A printed circuit board (PCB) featuring carved rectangular slots of 7.2 mm × 1 mm is designed to constrain the pattern and act as a stable foundation for the entire platform. To prevent tilting of the PZT plates and maintain electrical continuity with the PCB, 3D-printed joints with narrow slots measuring 7.1 mm × 0.22 mm are utilized. Hard plastic plates of identical size (7 mm × 7 mm × 0.2 mm) are employed as non-functional barriers surrounding the PZT units. This configuration preserves the barrier geometry around each unit, as every functional unit necessitates eight pieces of barriers with matching dimensions. For the STREAM prototype in this article, the distance between adjacent unit centers is set as 6 mm.

Each STREAM unit is assembled in a three-step process that begins with attaching a 3D-printed joint to the PZT plate and positioning it upright. Subsequently, the upright PZTs are inserted into the pre-cut slots on the PCB base plate so that the bottom part (2 mm) of the PZT is fixed with the PCB. To stabilize the entire

prototype, silver epoxy is applied to fill the blank spacer area from the backside. Finally, the prototype is submerged in the carrier fluid, which must possess a high density to support droplets of interest, excellent chemical stability, and low diffusion at the operating surface to minimize cross-contamination. The carrier fluid, Fluorinert™ FC-40, proves to be an excellent carrier fluid for our experiments due to its immiscibility in water, chemical inertness, and oxygen permeability. Its high density (1.86 g/mL) enables stable positioning of water-based droplets at the interface while minimizing cross-contamination between samples. For all the experiments in this article, the height of the carrier oil layer is set as 8 mm (i.e., 3 mm above the top of PZTs), and all the experiments are performed at room temperature and humidity.

When manipulating water-based droplets containing biological samples, the platform maintains reliable flow control and stable trapping characteristics. Due to the density difference between FC-40 and water, biological sample droplets are partially submerged in the carrier oil, typically to about half their height. This partial submersion, coupled with the surface tension at the oil–air interface, creates ideal conditions for manipulation. The droplets are adequately immersed to experience the hydrodynamic forces generated by the streaming vortices, while their surface exposure ensures stable positioning. Our experimental characterization confirms that droplets with dimensions smaller than the unit size (6 mm) can be precisely controlled without compromising the omnidirectional trapping characteristics of the platform<sup>53</sup>. The hydrodynamic forces generated by the streaming vortices provide sufficient strength to maintain precise control over droplet positioning and movement.

### Preparation of PDMS blocks

The PDMS unit blocks used in our experiments were fabricated through standard soft lithography techniques. We prepared the PDMS mixture by combining the prepolymer (Sylgard 184, Dow Corning) with its curing agent at a 10:1 weight ratio. Following thorough mechanical mixing, the mixture underwent vacuum degassing to remove all entrapped air bubbles. The degassed PDMS was then carefully poured onto a plastic master mold, and the entire assembly was thermally cured at 65 °C for 2 h. After complete curing, the PDMS layer was gently peeled off from the master mold and cut into rectangular blocks measuring  $\sim 3 \times 3 \times 1$  mm<sup>3</sup>.

### Input signal setup

During experiments, each STREAM unit is connected to one channel of a 16-channel functional generator via SMA cables. The 16-channel functional generator

consists of a stack of phase-synchronized functional generators (FeelTech FY-6600), and the system is controlled by MATLAB to perform dynamic control of the frequency and amplitude added to each channel (Supplementary Fig. 3a). For all the experiments in this article, we apply a processing time of 10 s, which is the time for the particles to be stabilized at one trapping point and the time between the successive refreshing of input voltages for all the channels.

### CNN calibration model

The calibration model contains three hidden layers, with the size of  $512 \times 1$ ,  $256 \times 1$ , and  $64 \times 1$ , respectively. The learning rate is set as  $10^{-5}$ , and Epoch is set as 300. For each hidden layer in the neural network, the activation functions are set as sigmoid, sigmoid, and ReLU, respectively. For each round of training, 10% of the training set is randomly selected for validation. The model's prediction accuracy shows spatial dependence, with higher accuracy achieved for positions farther from unit centers. This spatial variation in performance is partially attributed to hardware limitations in our current voltage control system (see the section "Discussion and conclusions" section). Despite these hardware constraints, the model maintains an average prediction error of around 0.5 mm across the majority of the operating area (as shown in Fig. 2f), enabling reliable particle manipulation for most applications.

### Training set and results capturing

To assemble the training set, each of the nine blocks in the STREAM prototype with  $2 \times 2$  units is scanned, with the voltage of each unit ranging from 8, 11, 14, 17, and 20 Vpp. Then, 300 input combinations of one or two adjacent units are added, resulting in a total training set size of  $9 \times 625 + 300 = 5925$  data points. For each input combination in the testing set, we use a 1 mm red polystyrene particle as the indicator of the trapping point and use a step time of 10 s to capture the actual stabilized position.

### Result capturing

The video data for both the training set and experimental results in Figs. 3–5 is captured by ProCam software using the camera on an Apple iPad, with the video mode set to VGA resolution ( $640 \times 480$  pixels) at 24 frames per second (Supplementary Fig. 3b). During experiments, the camera is mounted 30 cm above the STREAM platform at a fixed position using a standard laboratory support stand to ensure consistent imaging conditions for long-term recording. The field of view is adjusted to capture the entire  $4 \times 4$  unit array while maintaining sufficient resolution for accurate particle tracking.

### Video processing

We use a custom algorithm implemented in MATLAB (R2022a) to extract the actual position of the red polystyrene particle in each frame of the video data. The algorithm first applies the discrimination of different color channels in the RGB image using predetermined threshold values to isolate the red particle. After thresholding and binary image conversion, morphological operations are applied to remove noise and enhance particle detection. The centroid of the remaining binary object is calculated to determine the precise position of the particle's center at each specific frame. For each time step, we use the average position over the last 24 frames (corresponding to 1 s of video) as the stabilized position of the particle to minimize the impact of any transient fluctuations.

### Biocompatibility assessment

To evaluate the biocompatibility of the STREAM platform, we conducted a comparative study using K562 cells, a non-adherent human leukemia cell line widely used as a model organism in droplet-based microfluidics due to its non-adhesive properties. The cells were cultured in RPMI 1640 medium for 48 h and diluted to a concentration of  $10^6$  cells/mL. The sample was then divided into three 250  $\mu$ L droplets, each subjected to different environmental conditions: (1) standard cell culture conditions (37 °C, 5% CO<sub>2</sub>), (2) room environment, and (3) the STREAM platform. In the STREAM platform setup, as shown in Supplementary Fig. 4a, the droplet was kept in continuous rotation near the center of the prototype by activating the four central units with randomly varying inputs between 15 and 20 Vpp, refreshed every 10 min. Cell viability was monitored for 4.5 h across all three conditions. At 30 min intervals, a 5  $\mu$ L sample was extracted from each group and analyzed using a Countess II Automated Cell Counter. Each sample was measured in triplicate to obtain an average cell viability for that time point. The viability results are presented in Supplementary Fig. 4b. While the STREAM platform induced a slight decrease in viability of approximately 5%, it maintained a consistently high viability of ~90% over the extended period, demonstrating its biocompatibility for long-term manipulation of biosamples.

### Temporal response characterization

The temporal response of particle movement was characterized using the 105-step D-shaped routing demonstration shown in Fig. 3f. To quantify the stabilization dynamics, we analyzed two key aspects of the temporal response. First, we tracked the particle-to-target distance  $d_{\text{step}}$  versus time for each movement step. The results, presented in Supplementary Fig. 5a, show the

average distance trajectory with its associated variance across all steps. Our analysis reveals that particles typically converge to their target positions within approximately 9.5 s after applying new voltage combinations.

We further analyzed the distribution of stabilization times across all movement steps. The stabilization time ( $T_{\text{stabilize}}$ ) is defined as the duration required for a particle to remain within 20% of the total step distance from its target point. As shown in Supplementary Fig. 5b, while a small fraction of steps exhibit longer stabilization times, the majority of particles achieve stable positioning within 8 s. These results, combined with the time required for voltage switching between function generators, led to our implementation of a 10-s step time to ensure reliable and consistent particle positioning across different movement scenarios.

#### Acknowledgements

We acknowledge support from the National Institutes of Health (R01GM141055 and R01GM145960) and the National Science Foundation (CMMI-2104295).

#### Author contributions

H.Z. conceived the idea, led the experimental work, data analysis, and scientific presentation. W.Y. contributed to the theory, the experimental design, and the scientific presentation. H.Z. and N.P. wrote the article. T.J.H. provided overall guidance and contributed to the experimental design and scientific presentation.

#### Data availability

All data needed to evaluate the conclusions in the article are present in the main text and/or the Supplementary Materials. Additional data related to this article is available from the authors upon reasonable request.

#### Code availability

All codes related to this paper are available from the authors upon reasonable request.

#### Conflict of interest

T.J.H. has co-founded a start-up company, Ascent Bio-Nano Technologies Inc., to commercialize technologies involving acoustofluidics and acoustic tweezers.

**Supplementary information** The online version contains supplementary material available at <https://doi.org/10.1038/s41378-025-00907-5>.

Received: 4 October 2024 Revised: 25 January 2025 Accepted: 22 February 2025

Published online: 08 May 2025

#### References

- Dai, Y. J. et al. Zebrafish as a model system to study toxicology. *Environ. Toxicol. Chem.* **33**, 11–17 (2014).
- Chen, C. et al. Acoustofluidic rotational tweezing enables high-speed contactless morphological phenotyping of zebrafish larvae. *Nat. Commun.* **12**, 1118 (2021).
- Wagner, A., Duman, R., Stevens, B. & Ward, A. Microcrystal manipulation with laser tweezers. *Acta Crystallogr. Sect. D: Biol. Crystallogr.* **69**, 1297–1302 (2013).
- Smalyukh, I. I. et al. Optical trapping, manipulation, and 3D imaging of disclinations in liquid crystals and measurement of their line tension. *Mol. Cryst. Liq. Cryst.* **450**, 79/[279]–295/[295] (2006).
- Trivedi, R. P., Lee, T., Bertness, K. A. & Smalyukh, I. I. Three dimensional optical manipulation and structural imaging of soft materials by use of laser tweezers and multimodal nonlinear microscopy. *Opt. Express* **18**, 27658–27669 (2010).
- Yang, S. et al. Harmonic acoustics for dynamic and selective particle manipulation. *Nat. Mater.* **21**, 540–546 (2022).
- Yang, S. et al. Acoustic tweezers for high-throughput single-cell analysis. *Nat. Protoc.* **18**, 2441–2458 (2023).
- Tian, Z. et al. Wave number–spiral acoustic tweezers for dynamic and reconfigurable manipulation of particles and cells. *Sci. Adv.* **5**, eaau6062 (2019).
- Ao, Z. et al. Rapid profiling of tumor-immune interaction using acoustically assembled patient-derived cell clusters. *Adv. Sci.* **9**, 2201478 (2022).
- Yang, S., Kun, S., Min, Z., Hongjing, L. & Jianhua, Q. Effects of combined the fluid shear stress and tumor necrosis factor- $\alpha$  on cartilage phenotype in a dynamic microfluidic chip. *Chin. J. Chromatogr.* **35**, 458 (2017).
- Ali, M., Kim, W. & Park, J. Droplet microfluidic technologies for next-generation high-throughput screening. *Front. Lab. Chip Technol.* **2**, 1230791 (2023).
- Carnero, A. High throughput screening in drug discovery. *Clin. Transl. Oncol.* **8**, 482–490 (2006).
- Zang, R., Li, D., Tang, I.-C., Wang, J. & Yang, S.-T. Cell-based assays in high-throughput screening for drug discovery. *Int. J. Biotechnol. Wellness Ind.* **1**, 31 (2012).
- Grier, D. G. A revolution in optical manipulation. *Nature* **424**, 810–816 (2003).
- Chiou, P. Y., Ohta, A. T. & Wu, M. C. Massively parallel manipulation of single cells and microparticles using optical images. *Nature* **436**, 370–372 (2005).
- Chen, S., Li, Z., Liu, W., Cheng, H. & Tian, J. From single-dimensional to multidimensional manipulation of optical waves with metasurfaces. *Adv. Mater.* **31**, 1802458 (2019).
- Shen, Y. et al. Optical vortices 30 years on: OAM manipulation from topological charge to multiple singularities. *Light Sci. Appl.* **8**, 90 (2019).
- Blázquez-Castro, A. Optical tweezers: phototoxicity and thermal stress in cells and biomolecules. *Micromachines* **10**, 507 (2019).
- Rasmussen, M., Oddershede, L. & Siegmundfeldt, H. Optical tweezers cause physiological damage to *Escherichia coli* and *Listeria* bacteria. *Appl. Environ. Microbiol.* **74**, 2441–2446 (2008).
- Stroock, A. D. et al. Chaotic mixer for microchannels. *Science* **295**, 647–651 (2002).
- Kim, H., Min, K.-I., Inoue, K., Kim, D.-P. & Yoshida, J.-i. Submillisecond organic synthesis: outpacing Fries rearrangement through microfluidic rapid mixing. *Science* **352**, 691–694 (2016).
- Gossett, D. R. et al. Hydrodynamic stretching of single cells for large population mechanical phenotyping. *Proc. Natl. Acad. Sci. USA* **109**, 7630–7635 (2012).
- Paulsen, K. S., Di Carlo, D. & Chung, A. J. Optofluidic fabrication for 3D-shaped particles. *Nat. Commun.* **6**, 6976 (2015).
- Qasameh, M. A., Gervais, T. & Juncker, D. Microfluidic quadrupole and floating concentration gradient. *Nat. Commun.* **2**, 464 (2011).
- Harley, W. S., Kolesnik, K., Heath, D. E. & Collins, D. J. Enhanced acoustic streaming effects via sharp-edged 3D microstructures. *Lab Chip* **24**, 1626–1635 (2024).
- Zhang, L. & Marston, P. L. Acoustic radiation torque on small objects in viscous fluids and connection with viscous dissipation. *J. Acoust. Soc. Am.* **136**, 2917–2921 (2014).
- Gu, Y. et al. Acoustofluidic centrifuge for nanoparticle enrichment and separation. *Sci. Adv.* **7**, eabc0467 (2021).
- Ma, Z. et al. Spatial ultrasound modulation by digitally controlling microbubble arrays. *Nat. Commun.* **11**, 4537 (2020).
- Rogers, P. & Neild, A. Selective particle trapping using an oscillating microbubble. *Lab Chip* **11**, 3710–3715 (2011).
- Del Campo Fonseca, A. et al. Ultrasound trapping and navigation of micro-robots in the mouse brain vasculature. *Nat. Commun.* **14**, 5889 (2023).
- Liu, F.-W., Zhan, Y. & Cho, S. K. Propulsion reversal in oscillating-bubble powered micro swimmer. *J. Micromech. Microeng.* **31**, 084001 (2021).
- Kopitca, A., Latifi, K. & Zhou, Q. Programmable assembly of particles on a Chladni plate. *Sci. Adv.* **7**, eabi7716 (2021).
- Yiannacou, K. & Sariola, V. Controlled manipulation and active sorting of particles inside microfluidic chips using bulk acoustic waves and machine learning. *Langmuir* **37**, 4192–4199 (2021).
- Yiannacou, K. & Sariola, V. Acoustic manipulation of particles in microfluidic chips with an adaptive controller that models acoustic fields. *Adv. Intell. Syst.* **5**, 2300058 (2023).

35. Yiannacou, K., Sharma, V. & Sariola, V. Programmable droplet microfluidics based on machine learning and acoustic manipulation. *Langmuir* **38**, 11557–11564 (2022).
36. Kong, F., Yuan, L., Zheng, Y. F. & Chen, W. Automatic liquid handling for life science: a critical review of the current state of the art. *J. Lab. Autom.* **17**, 169–185 (2012).
37. Elrod, S. et al. Nozzleless droplet formation with focused acoustic beams. *J. Appl. Phys.* **65**, 3441–3447 (1989).
38. Trinh, E. Compact acoustic levitation device for studies in fluid dynamics and material science in the laboratory and microgravity. *Rev. Sci. Instrum.* **56**, 2059–2065 (1985).
39. Wixforth, A. et al. Flat fluidics: a new route toward programmable biochips. *Micromach. Microfabr.* **4982**, 235–242 (2003).
40. Guttenberg, Z. et al. Planar chip device for PCR and hybridization with surface acoustic wave pump. *Lab Chip* **5**, 308–317 (2005).
41. Collignon, S., Friend, J. & Yeo, L. Planar microfluidic drop splitting and merging. *Lab Chip* **15**, 1942–1951 (2015).
42. Gedge, M. & Hill, M. Acoustofluidics 17: Theory and applications of surface acoustic wave devices for particle manipulation. *Lab Chip* **12**, 2998–3007 (2012).
43. Wiklund, M., Green, R. & Ohlin, M. Acoustofluidics 14: applications of acoustic streaming in microfluidic devices. *Lab Chip* **12**, 2438–2451 (2012).
44. Reboud, J. et al. Shaping acoustic fields as a toolset for microfluidic manipulations in diagnostic technologies. *Proc. Natl Acad. Sci. USA* **109**, 15162–15167 (2012).
45. Rezk, A. R., Manor, O., Friend, J. R. & Yeo, L. Y. Unique fingering instabilities and soliton-like wave propagation in thin acoustowetting films. *Nat. Commun.* **3**, 1167 (2012).
46. Zhang, P. et al. Contactless, programmable acoustofluidic manipulation of objects on water. *Lab Chip* **19**, 3397–3404 (2019).
47. Liang, C. et al. Recent progress in flexible surface acoustic wave sensing technologies. *Micromachines* **15**, 357 (2024).
48. Ozcelik, A. et al. Acoustic tweezers for the life sciences. *Nat. methods* **15**, 1021–1028 (2018).
49. Rufo, J. et al. Acoustofluidics for biomedical applications. *Nat. Rev. Methods Prim.* **2**, 30 (2022).
50. Wu, M. et al. Sound innovations for biofabrication and tissue engineering. *Microsyst. Nanoeng.* **10**, 170 (2024).
51. Rufo, J. et al. A sound approach to advancing healthcare systems: the future of biomedical acoustics. *Nat. Commun.* **13**, 3459 (2022).
52. Matsuoka, C. Kelvin-Helmholtz instability and roll-up. *Scholarpedia* **9**, 11821 (2014).
53. Zhu, H. et al. Acoustohydrodynamic tweezers via spatial arrangement of streaming vortices. *Sci. Adv.* **7**, eabc7885 (2021).